Contrasting physical and chemical conditions of two rock glacier springs

Stefano Brighenti[1]*, Michael Engel[1], Monica Tolotti[2], Maria Cristina Bruno[2], Geraldene Wharton[3], Francesco Comiti[1], Werner Tirler[4], Leonardo Cerasino[2], Walter Bertoldi[5]

[1] *Faculty of Science and Technology, Free University of Bolzano/Bozen, Bolzano, Italy*
[2] *Department of Sustainable Agro-ecosystems and Bioresources, Research and Innovation Centre, Fondazione Edmund Mach (FEM), San Michele all'Adige (TN), Italy*
[3] *School of Geography, Queen Mary University of London. London, United Kingdom*
[4] *ECORESEARCH S.r.l., Bolzano, Italy*
[5] *Department of Civil, Environmental and Mechanical Engineering, University of Trento, Trento, Italy*

*Corresponding Author: Stefano Brighenti. Piazza Università 5, Faculty of Science and Technology, Free University of Bolzano/Bozen, Italy. Mobile: +39 3474806941. E-mail: stefano.brighenti@alumni.unitn.it

Running title: Contrasting rock glacier springs

Key words: mountain permafrost, solute export, hydrochemistry, European Alps, trace elements, alpine springs, wavelet analysis, climate change

Abstract

Rock glaciers are increasingly influencing the hydrology and water chemistry of Alpine catchments. During three consecutive summers (2017-2019), we monitored by recording probes and fortnightly/monthly field campaigns the physical and chemical conditions of two rock glacier springs (ZRG, SRG) in the Zay and Solda/Sulden catchments (Eastern Italian Alps). The springs have contrasting hydrological conditions with ZRG emerging with evident ponding (pond-like), and SRG being a typical high-elevation seep (stream-like). Water temperature was constantly low (mean 1.2 °C, standard deviation 0.1 °C) at both springs. Concentrations of major ions (dominated by SO_4^{2-}, HCO_3^-, Ca^{2+} and Mg^{2+}) and trace elements (As, Sr, Ba, U, Rb) increased, and water became more enriched in heavy stable isotopes ($\delta^{18}O$, δ^2H) towards autumn. This solute and isotopic enrichment had an asymptotic trend at SRG, and a unimodal pattern at ZRG, where peaks occurred 60-80 days after the snowmelt end. Wavelet analysis of electrical conductivity (EC) and water temperature records revealed daily cycles only at SRG, and significant weekly/biweekly fluctuations at both springs attributable to oscillations of meteorological conditions. Several rainfall events triggered a transient (0.5-2 hrs) EC drop (of 5-240 µS cm^{-1}) and water temperature rise (of 0.2-1.4 °C) at SRG (dilution and warming), whereas only intense rainfall events occasionally increased EC (by15-85 µS cm^{-1}) at ZRG (solute enrichment and thermal buffering), with a long-lasting effect (6-48 hrs). Building on previous research, we suggest that rock glacier springs with differing flow conditions, i.e., stream-like and pond-like, have contrasting fluctuations of water parameters at different timescales. Thus, for pond-like springs, peaks of EC/solute concentrations might indicate a seasonal window of major permafrost thaw. Our quantitative description of the hydrochemical seasonality in rock glacier outflows and the physical and chemical response to precipitation events provides relevant information for water management in mountain areas under climate change.

1. INTRODUCTION

Climate change is having a profound effect on the quantity and quality of Alpine freshwaters, as the diminishing hydrological contribution from receding glaciers (Intergovernmental Panel on Climate Change [IPCC], 2019) is paralleled by an increased influence from paraglacial and periglacial landforms (Haeberli, Schaub, & Huggel, 2017; Brighenti et al., 2019a). In particular, rock glaciers (i.e., creeping bodies of rock fragments providing evidence of mountain permafrost) have been addressed as significant water reservoirs at a global scale (Jones, Harrison, Anderson & Betts, 2018) as their subsurface ice melts much more slowly than that of glaciers (Haeberli et al., 2017). Their hydrological importance is also promoted by an increasing storage capacity made available by the loss of internal ice (e.g., Wagner, Pauritsch & Winkler, 2016; Jones, Harrison, Anderson & Whalley, 2019). In fact, the internal structure of rock glaciers influences their hydrological behaviour. Growing evidence suggests the importance of a fine-grained basal layer with low hydraulic conductivity, which constitutes a groundwater storage system in these landforms. This sub-permafrost layer exerts a major control on base flow conditions, with fractures and depressions occurring in the basal bedrock only playing a minor role (Jones et al., 2019; Wagner, Brodacz, Krainer & Winkler, 2020). Most of the rainwater is quickly exported from rock glaciers across lateral flows in the supra-permafrost layer, which is made of coarse blocky materials with high hydraulic conductivity. The presence of fractures and ice-free areas in the ice-sediment matrix allows some water to cross the intra-permafrost zone, enhancing the recharge of the sub-permafrost aquifer (Wagner et al., 2020). This mixed water contribution can support surficial waters emerging as lakes, ponds, or streams at the rock glacier forefields.

The seasonal snowmelt is a key hydrological driver of rock glacier springs. In fact, their discharge is higher during early summer, and decreases towards autumn as the snow on the rock glacier and its catchment progressively melts away (e.g., Krainer & Mostler, 2002; Colombo et al., 2018a). During late summer/autumn, only a small fraction of discharge (< 5 %, e.g., Krainer, Chinellato, Tonidandel & Lang, 2011) can be sustained by internal ice melt (Colombo et al., 2018b; Jones et al., 2019), which strongly influences the hydrochemistry of rock glacier springs. Long-term studies on headwaters fed by rock glaciers attributed the increase of electrical conductivity (EC) and concentrations of major ions and trace elements observed in the last decades, to the progressive permafrost thawing (e.g., Thies et al., 2007; Colombo et al., 2018b; Steingruber, Bernasconi & Valenti, 2020). The seasonal timing of solute export from rock glaciers is particularly important. In fact, high concentrations of metals and metalloids have been observed in rock glacier springs, often exceeding drinking water and environmental quality standards (Nickus & Thies, 2015; Brighenti et al., 2019b), and affecting the water chemistry further downstream along the river network (Brighenti et al., 2019a). Solute concentrations typically increase during late summer because the contribution of diluting snowmelt decreases, and those of reacted groundwater and permafrost ice melt increase (Williams, Knauf, Caine, Liu, & Verplanck, 2006; Caine, 2010; Krainer et al., 2015; Colombo et al., 2018a; Munroe, 2018). Different studies revealed contrasting patterns of solute increase in rock glacier springs, reporting either an asymptotic behaviour of EC/solute concentrations with the plateau corresponding to autumn and winter (Krainer, Mostler, & Spötl, 2007; Krainer et al., 2015; Nickus & Thies, 2015; Harrington,

Mozil, Hayashi & Bentley, 2018), or a unimodal trend with late summer peaks (Colombo et al., 2018a). However, the drivers of these contrasting seasonal trends have yet to be investigated. Even the influence of precipitation on rock glacier hydrochemistry is still being debated. Colombo et al. (2018a) found intense rainfall events caused solute-enrichment in a rock glacier pond whereas most studies reported a dilution effect from rainfall with transient solute-depletion in rock glacier streams (e.g., Krainer & Mostler, 2002; Berger, Krainer, & Mostler, 2004; Krainer et. al., 2007; Harrington et al., 2018).

Rock glaciers are efficient thermal buffers, and for this reason they represent potential climate refugia for cold-adapted terrestrial and aquatic organisms under global warming (Brighenti et al., 2021). Springs fed by intact rock glaciers are typically very cold (< 2 °C), which testifies to the occurrence of permafrost (Carturan et al., 2016). The snow and the internal ice release latent heat when melting, and cool down infiltrating rainwater (e.g., Krainer & Mostler, 2002; Krainer et al., 2007; Millar, Westfall, & Delany, 2013; Krainer et al., 2015; Harrington, Hayashi, & Kurylyk, 2017; Munroe, 2018). In fact, rainfall events can either trigger transient drops of water temperature (T_{water}; Geiger, Daniels, Miller, & Nicholas, 2014; Krainer et al., 2015; Winkler et al., 2016; Colombo et al., 2018a; Harrington et al., 2018), or have no thermal effect (Krainer & Mostler, 2002; Krainer et al., 2007) on rock glacier outflows during the snow free period. However, quantitative analyses aimed at understanding the main parameters driving intensity, duration, and temporal patterns of the response of T_{water} and solute concentrations to precipitation events are still lacking. Rainfall events can also disrupt the diel fluctuations of water parameters in rock glacier springs. These oscillations typically occur during the seasonal snowmelt, and smooth down as summer progresses (Krainer & Mostler, 2002; Berger et al., 2004; Krainer et al., 2007). Periodic fluctuations of EC and T_{water} might also occur over longer timescales (e.g., associated with switching warm and cold periods) but quantitative assessments of such oscillations have been never attempted.

In this study, we investigated the physical and chemical conditions of two rock glacier springs in a deglaciating area of the Eastern European Alps (Solda/Sulden valley) during three consecutive summers (2017-2019). The springs originate from two different rock glaciers with contrasting hydromorphological settings. We addressed three major hypotheses:

- H1) time elapsed after snowmelt ends has a strong control on the solute dynamics of both springs (i.e., enrichment towards autumn);
- H2) amplitude of EC and T_{water} diel cycles is larger during the snowmelt period, and decreases with increasing time elapsed after the snowmelt end;
- H3) precipitation events trigger transient responses of EC, and the intensity and duration of this response are controlled by the intensity and duration of precipitation events.

2. STUDY AREA

We studied the permanent springs emerging from two tongue-shaped rock glaciers located in distinct subcatchments (Zay and Solda/Sulden) of the upper Solda/Sulden catchment, Eastern Italian Alps (Figure 1; Table 1). The geographical, climatic, geological, and hydrological

settings of the catchment are described in Engel et al. (2019) and Brighenti et al. (2019a). Geologically, the area belongs to the Austroalpine domain, represented by a crystalline basement and its sedimentary cover (Montrasio et al., 2015; Table 1). Although the ice abundance and distribution of these rock glaciers is unknown, the two landforms are classified as intact (i.e., containing ice) by Kofler et al. (2020), in agreement with the rock glacier inventory of the Autonomous Province of Bolzano/Bozen [APB] (2020a) which classified both landforms as active (i.e., intact and with motion). Oversteepened fronts with unstable boulders, localised scouring, and sparse/absent vegetation suggest the occurrence of creeping activity for both rock glaciers, but no detailed studies exist on their kinematic behaviour.

The Zay spring (ZRG) is five meters wide, and it originates with an evident ponding from the south-western side of the Zay rock glacier terminus. In part, this rock glacier is hydrologically connected with the Ausserer Zay glacier, whose front is located ~0.5 km away from the rock glacier upstream margin, and the glacier-fed stream flows parallel to the rock glacier along its northern margin (APB, 2020a; see Supplementary 1).

The Sulden spring (SRG) is ~30 cm wide, and it originates as a typical mountain seep from the Sulden rock glacier, which is composed of two merged bodies and is partially reshaped by an unsealed road at its terminus (APB, 2020a; Supplementary 1). The spring lies 40 m downstream from the western side of the rock glacier front, and it partially drains moraine deposits (Supplementary 1). To distinguish the two rock glacier outflows according to their distinct water flow conditions, we hereafter define them as pond-like (ZRG) and stream-like (SRG) springs.

Two automatic weather stations managed by the APB were used to retrieve meteorological data. The Madriccio/Madritsch station (2825 m a.s.l.) is located within the same glacial cirque as SRG, at a distance of 1.4 km and an elevation 232 m higher. A second weather station is located in the Solda/Sulden village (1900 m a.s.l.), and it was used to validate precipitation data for the Zay spring (see section 3.2). The Madriccio/Madritsch station is located 5.6 km away from ZRG and at a 133 m higher elevation, and it is separated from the Zay subcatchment by the Rosim subcatchment (Figure 1A).

3. MATERIALS AND METHODS
3.1. Field activities and laboratory
The two springs were investigated during three consecutive summers (2017-2019). Recording probes for EC and T_{water} (HOBO U24, ONSET, MA, USA; 5 μS cm^{-1} and 0.1 °C accuracies; HOBO Pendant UA-001-08, ONSET, MA, USA; 0.45 °C accuracy), recording at 30 min (2017, 2018) or 15 min (2019) intervals, were deployed during the snowmelt period (i.e., before the vanishing of the seasonal snow cover), and retrieved in September/October each year during the flow recession period. EC was not recorded at ZRG during 2017 because the recording probe was unavailable. Each data-logger was deployed at the same location every year, as close as possible to the rock glacier terminus (see Supplementary 1 for their exact locations).

During each sampling campaign, we measured T_{water}, EC, and turbidity with portable probes (Cond-3310 and Turb-430IR, WTW, Germany), and collected water samples for

laboratory analyses on a monthly basis during 2017 and 2018, and bi-weekly in 2019 (Figure 1F). Samples for the assessment of base chemistry were collected in clean 500 mL polyethylene bottles, stored in the dark at 4 °C until delivery within two to three days to the Hydrochemistry laboratory of the Edmund Mach Foundation (San Michele all'Adige) for the measurement of Alkalinity, pH, HCO_3^-, Ca^{2+}, Mg^{2+}, Cl^-, Na^+, K^+, total nitrogen (TN), NH_4^+-N, NO_3^--N, total phosphorus (TP), PO_4^{3-}-P, SO_4^{2-} and SiO_2, following standard methods (Baird & Bridgewater, 2017). Additional stream water was filtered through cellulose acetate membranes (0.45 µm pore diameter) into 100 mL polyethylene bottles (previously washed with > 65% HNO_3), acidified in the field (1.5 % volume, > 65% HNO_3), and delivered to the Ecoresearch S.r.l. laboratory (Bolzano/Bozen) where element concentrations (Be, B, Al, Ti, V, Cr, Mn, Fe, Co, Ni, Cu, Zn, As, Se, Rb, Sr, Mo, Ag, Cd, Sn, Sb, Ba, Tl, Pb, U, Bi) were measured with Inductively Coupled Plasma Mass Spectrometry (ICP-MS ICAP-Q, Thermo Fischer® Scientific, MA, USA). To disentangle the contribution of different water sources to spring discharge, we collected: (i) snowmelt water (dripping from snow patches); (ii) glacier ice melt (from the Zayferner rivulets during glacier ablation); (iii) precipitation (integrated monthly samples of May to October; rainwater containers placed nearby SRG and ZRG and built following IAEA, 2014); and (iv) spring water in 50 ml polyethylene bottles. These samples were stored at 4 °C and analysed by a laser spectroscope (Picarro L2130i, CA, USA) at the Free University of Bolzano/Bozen laboratory for the determination of δ^2H (0.1 ‰ precision) and $\delta^{18}O$ (0.025 ‰ precision).

3.2. Data analysis

We used the meteorological data recorded by the two automatic stations (1st January 2016 to 31st December 2019; APB, 2020b). We considered the following parameters: snow height (cm, 10 min resolution), precipitation (mm, 5 min), air temperature (T_{air}, °C; 10 min) at the Madriccio/Madritsch station; precipitation (mm) and T_{air} (°C) at the station of the Solda/Sulden village (same time resolution as for Madriccio/Madritsch). This dataset was elaborated to ensure consistent interval records of water parameters (i.e., 30 min intervals during 2017 and 2018, 15 min intervals during 2019). Based on the Madriccio/Madritsch station, we quantified the meteorological conditions in the area, and estimated for each year the end of the snowmelt period, defined as the date from which the winter snow cover was absent (< 0 cm) for at least seven consecutive days. Based on this date, we calculated for each sampling date the variable "days after the snowmelt", that we used as a proxy to describe the seasonal patterns of water parameters while accounting for the contrasting end of the snowmelt period among different years.

A Principal Component Analysis (PCA) was performed to visualize the physical and chemical parameters characterizing the two springs and their seasonality. We used the R package *factoMiner* (Husson, Josse, Le & Mazet, 2020) which automatically applies variables standardisation (scaling and centering), and the *factoextra* (Kassambara & Mundt, 2020) and *corrplot* (Wei et al., 2017) R packages for data visualisation. $\delta^{18}O$ was discarded a-priori from PCA analysis because it was strongly collinear with δ^2H.

The relationship between precipitation events and the variation of water parameters was estimated by determining new variables from the physico-chemical and meteorological

dataset. For each precipitation event (minimum intensity ≥5 mm h^{-1} over the recorded interval), we calculated the following parameters: total precipitation (mm); duration (hrs); and the average and maximum intensity (mm hr^{-1}) of precipitation. The minimum inter-event time (to consider two separate precipitation events) was set at 1 hr, as suggested by Molina-Sanchis, Làzaro, Arnau-Rosalén, & Calvo-Cases (2016). The type of precipitation was estimated for each event as a function of the liquid-solid state of water, based on the average air temperature during the event (US Army Corps of Engineers; 1956): rainfall ($T_{air} > 3$ °C), rainfall/snow (1 °C $\leq T_{air} \leq 3$ °C), snow/rainfall (-1 °C $\leq T_{air} < 1$ °C) or snow ($T_{air} < -1$ °C). We could use the weather dataset of the Madriccio/Madritsch station also for the analyses at ZRG (located in an adjacent subcatchment) because all precipitation events associated to responses in EC/T_{water} at this spring were also recorded by the Solda/Sulden weather station (located at the Zay closing section), and as such could be considered as catchment scale events.

When a transient shift (δ) above the instrumental accuracy of T_{water} (> 0.1 °C) and/or EC (> 5 μS/cm) was detected (for T_{water} we used the records of HOBO Pendant UA-001-08, with lower accuracy, only when the U-24 was not recording, i.e. during 2017 and June/July 2018), we calculated the following weather variables: lag time (hrs) between the onset of the precipitation event and the onset of the response; variation of EC (δEC = EC minimum/maximum – EC at the precipitation onset); variation of T_{water} (δT = T_{water} minimum/maximum – T_{water} at the precipitation onset); δEC and δT duration (hrs; time elapsed to return to pre-event values or to the trend of the corresponding cycles, assessed by visual inspection of EC and T_{water} plots).

To estimate the drivers and temporal trends of water parameters we used a combination of Linear Models (LM), Generalised Linear Models (GLM) and Generalized Additive Models (GAM) that were performed using the basic R functions (for LM, GLM) or the package *mgcv* (for GAM; Wood, 2020) in R 4.0.0 (R Development Core Team, 2020). To identify trends in the recorded time series we applied GAMs separately for each station, assuming daily averages of T_{water} and EC as response variables, days after the snowmelt as an explanatory variable, and year as covariate. Moreover, to prevent heterogeneity of residuals, we discarded some outliers in the series before running the GAM analyses, following Zuur et al. (2009). We also used LM, GAM, and GLM to identify the drivers of the physical and chemical response to precipitation events, separately for each station, by setting the absolute variations in the parameters (δEC, δT, δEC duration, δT duration) as response variables and the parameters of precipitation (total precipitation, intensity, maximum intensity, days elapsed after the snowmelt) as predictors, and precipitation type as categorical covariate. We validated the models with residual graphs and following the procedures outlined by Zuur et al (2009). The distribution family (Gaussian or Gamma) of GAM/GLM was selected based on the Akaike Information Criterion (Zuur et al., 2009). Thin plate regression spline is the default smoother used for GAM in the *mgcv* package (Wood, 2020).

The periodicity in T_{water} and EC time series was analysed with wavelet analysis. This spectral analysis investigates periodical phenomena in time series by partitioning the variability in the series into different components according to different frequencies (Morlet, Arens, Fourgeau, & Giard, 1982). We applied Morlet wavelet transformation with the R

WaveletComp package v1.1, which automatically standardises the data after detrending (Rösch & Schmidbauer, 2018). The statistical significance (p ≤ 0.01) of different periods was estimated by comparing the actual spectrum against a white noise (random) distribution. The expectation of the power spectrum at each time and scale is based on the series variance (Rösch & Schmidbauer, 2018). We applied separate analyses for each station, year, and parameter. With the same package, we also analysed wavelet coherence among T_{water}, EC, T_{air} and global radiation to detect consistent fluctuations and phase coherence among these variables.

We visualised the isotopic dataset in a dual plot, where we fitted the global (GMWL) and the local (LMWL) meteoric water lines. We used the LMWL regression parameters to estimate the line-conditioned excess of all water samples (lc-excess; Landwehr & Coplen, 2006).

We tested for statistical differences in the physical and chemical variables between the two springs by Mann-Whitney test (U-statistics). We used this non-parametric test because most of the data were not normally distributed (Shapiro-Wilk test, $p < 0.05$), and/or because variances were significantly uneven between groups (Levene's test, $p < 0.05$), even after data transformation. We used the software SPSS (v.25, IBM, 2018) to carry out these statistical analyses.

4. RESULTS
4.1. Climatic conditions during the monitoring period
During the three years of monitoring, the Madriccio/Madritsch station recorded typical alpine conditions, with a mean air temperature of -1.2 °C and winter snow cover lasting for 206-222 days (Figure 1F). An early onset of snow accumulation occurred in 2016 (10th October) when compared with 2017, 2018 (late October) and 2019 (mid-November). In 2017 there was an earlier end to the snowmelt (10th June) compared to 2018 (16th June) and 2019 (29th June). Summer 2017 was warmer (August air temperature = 8.6 ± 3.9 °C) and wetter (total precipitation during the snow free period equal to 506 mm) than the summers of 2018 (7.5 ± 3.3 °C; 390 mm) and 2019 (7.8 ± 2.9 °C; 504 mm).

4.2. Hydrochemistry and tracers
At both springs, water temperature was very low and constant over the entire monitoring period (1.2 ± 0.1 °C), and SO_4^{2-}, Ca^{2+}, HCO_3^- and Mg^{2+} were the dominant ions (Supplementary 3). At the stream-like spring (SRG), EC values and SO_4^{2-}, Ca^{2+}, HCO_3^-, Mg^{2+} and K^+ concentrations were significantly higher (U > 41, p ≤ 0.002), and turbidity was significantly lower (U = 311, $p < 0.001$) than at the pond-like spring (ZRG). Concentrations of the other ions did not significantly differ between the two springs. Concentrations of As, Sr, and Ba were significantly higher (U > 105, $p < 0.001$), and those of Rb significantly lower (U = 240, $p < 0.001$) at SRG, whereas Al, Mn, Fe, Ni, Cu, Zn, Se, Mo, Pb and U did not significantly differ between the two springs. Ag, Cd, Sn, Sb, Tl, Bi, Cr, V were very close to or below detection limits (Supplementary 2, 3).

The first two axes of the PCA explained 72.2 % of the total variance within the dataset (Figure 2, Table 2). The gradient along PC1 separated the samples from the two stations, with

SRG being in general more solute-enriched. Sample scores spread on a seasonal gradient along PC1 for both stations but only for ZRG along PC2. Both springs exhibited isotopic enrichment, increasing T_{water}, EC, and concentrations of major ions, silica, and trace elements as a function of the days elapsed after the snowmelt period, yet with contrasting patterns (Table 3, Figure 3, 4). At SRG, solute concentrations exhibited a linear increase and the isotopic enrichment had an asymptotic behaviour over the time gradient. In contrast, ZRG showed a positive unimodal trend for these parameters, with peaks corresponding to 60-80 days after the end of the snowmelt (i.e., early September; Figure 4).

Water samples from both springs plotted along the GMWL on a dual isotope plot (Figure 3A). Values of δ^2H and $\delta^{18}O$ in spring water samples were significantly lower than in precipitation (U > 142, p < 0.001), and were not significantly different from melting snow and glacier ice melt (p ≥ 0.28). Values of δ^2H, $\delta^{18}O$, and lc-excess were lower at ZRG than at SRG for each sampling occasion (Figure 3B, 3C). As summer progressed, spring water became increasingly enriched in heavy isotopes, shifting from the signals of melting snow and ice to those of precipitation (Figure 3).

4.3. Trends of water parameters at multiple timescales
The continuous monitoring of EC and T_{water} revealed contrasting patterns for the two springs during the study period (Figure 5A). GAM analysis confirmed the importance of the days after the snowmelt as a significant explanatory variable (Figure 5B, Table 3). Seasonal minima in T_{water} were recorded during the snowmelt period at both stations. As summer progressed, water temperature showed a positive unimodal behaviour at the stream-like spring (SRG), peaking during mid-summer, and a continuous increase at the pond-like spring (ZRG). In contrast, EC continuously increased at SRG and had a positive unimodal behaviour at ZRG, where peaks occurred during late summer before the autumn decline (Figure 5A).

Wavelet analysis showed distinct cycles in the T_{water} and EC series at the two springs (Figure 6). For SRG one-day cycles and one-, eight- to 16-day cycles, respectively, were displayed. The most intense daily fluctuations were detected during the snowmelt period, when both water parameters had late evening minima and mid-day maxima (0.1-0.2 °C and 20-70 µS cm^{-1} fluctuation ranges). The intensity of EC fluctuations at SRG progressively smoothed over the summer (e.g., 10-30 µS cm^{-1} during August), whereas T_{water} had a unimodal trend with larger oscillations (0.2-0.3 °C), albeit close to the instrument precision, during August. Daily oscillations of water parameters occurred earlier in the day as summer progressed (e.g., mid-day maxima and early evening minima), and ceased during September (Figure 6). In contrast, daily fluctuations were absent at ZRG, where T_{water} had primary 16-day (0.4 °C fluctuations) and secondary 5-day fluctuations (0.1-0.2 °C), and these oscillations persisted during the entire summer. For EC, cycles were detected at ZRG from mid-August, with six to eight-day primary and 16-day secondary fluctuations (of 10-144 µS cm^{-1}), and displaying a higher intensity during early September. The bivariate time series of T_{water} and T_{air}/global radiation revealed coherent fluctuations at different timescales for both springs, but these were only in phase at SRG in early summer (i.e., during the snowmelt; Supplementary 3). Periods of precipitation, snow cover presence and/or cold air conditions recorded at the Madriccio/Madritsch station after the end of the seasonal snowmelt

corresponded to the major interruptions of the diel cycles in T_{water} and EC at the rock glacier springs (Figure 6).

4.4. Effect of precipitation events

The two springs showed contrasting responses to precipitation events. The analysis of the time series at the Madriccio/Madritsch station over the three summers detected 218 precipitation events.

At SRG, only one snow/rainfall event (from a total of N = 18), 19 rainfall/snow events (N = 38) and 40 rainfall events (N = 145) were associated with a response in EC and/or T_{water}. Almost 94 % of rainfall or rainfall/snow events > 2 mm occurring when snow cover was absent were associated with a negative response in EC and a positive response of T_{water} (larger than the instrument accuracy). Total precipitation was the best predictor for the response of EC and T_{water} at the two springs in GLM analyses, and also gave the best performance (explained deviance) when periods of snow cover presence were excluded from the analysis. During snow-free periods, we observed a low fall in EC (of 5.5-11.1 μS cm^{-1}) to precipitation events down to a threshold of around 5 mm, after which δEC declined as a function of total precipitation (Figure 5A, Figure 7, Table 3). Models revealed that the response of T_{water} to precipitation events was most likely to occur for the events during relatively warm conditions (T_{air} > 4 °C) and when snow cover was absent. The delay between precipitation onset and the associated response in T_{water} and EC ranged between 30 min and 2.5 hrs.

At ZRG, only seven precipitation events influenced T_{water}. The response was weakly negative and close to the instrument accuracy (-0.2 < δT < -0.1 °C), long-lasting (1-2 days), and it was only recorded from late July to early September. We found no relationship between the meteorological parameters and δT. Only 9 (total N = 96) precipitation events influenced EC with values above the instrument accuracy. These events occurred during relatively warm conditions (T_{air} > 4 °C) and when snow cover was absent. δEC was positive and exponentially related to total precipitation (R^2 = 0.79, p = 0.001), as also shown by GAMs (Figure 7, Table 3). The δEC lag-time ranged from 6-9.5 hrs (except 2 hrs on one occasion), and we found no relationship between precipitation duration and δEC duration.

5. DISCUSSION

The two springs investigated in this study are typical examples of rock glacier outflows but, despite exhibiting many common features, they display significant differences in hydrochemistry and seasonal trends of water parameters. In these ways, they embody the contrasting hydrochemical patterns that can be found in the literature on rock glacier hydrology.

5.1. Snow and permafrost drive spring similarities

As outflows from intact rock glaciers, the two springs have comparable physical and hydrochemical attributes. They have very cold waters with only small fluctuations in temperature on a daily and seasonal basis, their chemistry is dominated by sulphates, calcium, magnesium and carbonates, and a sharp solute enrichment occurs during late summer under

the coupled influence from reacted groundwater and permafrost (see Jones et al., 2019). It has long been recognized how snowmelt is a major hydrological driver in alpine settings (Khamis, Brown, Milner, & Hannah, 2015), and we normalised the interannual variability in the snowmelt timing by analysing the seasonal trends of water parameters as a function of the days elapsed after seasonal snow cover disappeared. In particular, our results fully support the first hypothesis (H1) of a solute enrichment occurring at both springs after the snowmelt end towards autumn. Meteorological variability influences the thermal conditions of rock glaciers, and thus their hydrological behaviour (Colombo et al., 2018a). For example, an anticipated snow accumulation precludes the efficient cooling of the active layer during winter (thermal buffering of snow against cold air), whereas an anticipated snowmelt, and warm summers, accelerate the warming of the active layer and promote ice melting (Schoeneich et al., 2011). In fact, while the snowmelt water typically has very low solute concentrations (e.g., Engel et al., 2019) and as such promotes water dilution during early summer, permafrost ice is enriched in solutes and its thawing enhances solute concentrations in the water during late summer (Colombo et al., 2018b). Thus, we attribute the higher EC and concentrations of major ions and trace elements detected at both springs during late summer 2017 to a higher ice melt contribution compared with summers 2018 and 2019. Summer 2017 had an earlier end of the snowmelt period, warmer atmospheric conditions, and a higher amount of rainfall when compared with summers 2018 and 2019. Furthermore, the earlier onset of winter snow accumulation in 2016 when compared with 2017 and 2018, helped maintain the rock glacier in warmer winter conditions.

5.2. Lithology and geomorphology drive spring differences

Despite these similarities, the two rock glacier springs differed in several hydrochemical parameters and in their seasonal behaviour. The hydrological connection between the Zay rock glacier and the glacier located upstream (Brighenti et al., 2019a) explains the higher turbidity values (peaking in the seasonal period of glacier ablation), the more depleted isotopic signal, and the lower concentrations of major ions recorded at the Zay spring when compared with the Sulden spring. The different bedrock composition of the two rock glaciers can explain the distinct concentrations of major ions and trace elements in the two springs. These differences progressively decline towards autumn, when the baseflow contribution becomes the dominant component of rock glacier discharge (Wagner et al., 2020). Although some studies did not find evidence of a lithological origin of high trace element concentrations in rock glacier waters (Thies et al., 2007; Krainer et al., 2011), and some attributed solute export from permafrost thawing to the release of legacy contaminants (Scapozza et al., 2020), rock weathering is considered the major driver of trace element export in rock glacier waters. This is especially under permafrost thawing conditions (Colombo et al., 2018b) when variations in the availability of weathering products results in the preferential export of different combinations of solutes (Steingruber et al., 2020; Tolotti et al., 2020). In fact, rubidium and uranium had higher concentrations at the Zay spring, where the latter element exceeded up to four times the limits for drinking water and environmental quality standards (as no limits for the European Union [EU] exist, we here refer to the United States Environmental Protection Agency [EPA], 2018) during late summer, and these

elements are typical minor constituents of the orthogneisses of the Zay catchment (Mair, pers. comm., 2019). In contrast, concentrations of arsenic, barium, and strontium were much higher at the Sulden spring, where the bedrock is enriched in these elements (Engel et al., 2019). Notably, arsenic concentrations were high, exceeding by two to four times the limits for drinking water quality (EU, 2020), but did not show a clear seasonality. This suggests that permafrost thawing does not enhance arsenic concentrations, which instead might originate from the weathering of the calcareous bedrock filling the cracks in this area of tectonic contact (Montrasio et al., 2015). In fact, a recent study attributed the origin of arsenic in rock glacier waters to the presence of As-enriched carbonate ores associated with quartz dykes (Eder, 2019).

The two springs have different fluctuations of water parameters at multiple timescales. This was detected by wavelet analyses, used in this study for the first time to investigate rock glacier hydrology. Diel cycles of EC and water temperature were only detectable at the Sulden stream-like spring, where they were particularly evident during the snowmelt period (i.e., before and immediately after the calculated end of the snowmelt) and smoothed out as summer progressed. This agrees with other studies on rock glacier springs that pointed to the importance of snowmelt cycles in driving the oscillations of water parameters (Krainer & Mostler, 2002; Berger et al., 2004; Krainer et al., 2007). The absence of diel cycles at the Zay pond-like spring is possibly due to the rock glacier body, that may be very efficient in buffering the snowmelt cycles occurring at its surface because of the smoothing effect from massive rocky debris. Also, translatory flow mechanisms occurring in the rock glacier interior might offset the potential fluctuations of water parameters (see paragraph 5.5). Thus, there is not clear support for the second hypothesis (H2) on the presence of clear diel cycles of water parameters in rock glacier springs as these fluctuations were only evident for the Sulden stream-like spring. However, wavelet transformations detected fluctuations at weekly to bi-weekly timescales, suggesting that both rock glaciers are hydrochemically and thermally responsive to the medium-term meteorological variability typical of the alpine summer.

5.3. A window of permafrost thaw revealed by water parameters?

The contribution from permafrost ice melt in rock glacier outflows is more likely to occur in the late summer, when the 0 °C isotherm reaches the interstitial ice and triggers partial melting (Williams et al., 2006; Leopold et al., 2011; Colombo et al., 2018a). At the Sulden rock glacier, the increased permafrost ice melt contribution might have caused the onset of water temperature decline and the solute enrichment at the end of August/early September each year during the study period. The behaviour of water temperature resembles that previously reported for active (Krainer & Mostler, 2002; Krainer et al., 2007; Krainer et al., 2015; Munroe, 2018) and inactive (Harrington et al., 2018) rock glaciers, as well as for periglacial taluses (Millar et al., 2013). In contrast, the steady increase of water temperature at the Zay pond-like spring suggests a slow thermal response of the rock glacier to the degree-days previously accumulated over the season. At this spring, EC and solute concentrations had a unimodal trend, peaking 60-80 days after the snowmelt end. Similar timings of maximum EC and solute concentrations were also detected by studies on ponds influenced by rock glaciers (Colombo et al., 2018a) and permafrost (Colombo et al., 2019),

and may reveal the period of permafrost thaw. This "window of permafrost thaw" ends when the cold air and the declining solar radiation promote the re-cooling of the active layer in autumn and prevent further internal ice melting. The isotopic enrichment occurring during the same period at the Zay pond-like spring might reveal the release of water from permafrost ice melt that has undergone several freeze/thaw cycles (Williams et al., 2006), and/or a higher contribution from liquid precipitation, which was isotopically more enriched when compared with the spring water.

At the Sulden stream-like spring, the window of permafrost thaw might be identified differently. In the late summer, any solute enrichment occurring during this period (at least, during dry days), while isotopic values do not change, cannot be attributed to the concentration-effect, and might reveal permafrost ice melt. Unfortunately, discharge was not monitored in our study, and this hypothesis thus remains speculative and should be tested in future research.

5.4. Contrasting responses to rainfall events

Several precipitation events which occurred during the monitoring period triggered a transient response of EC at the two springs. The variations were more marked when the snow cover was absent, precipitation was very likely in the form of rainfall, and precipitation amounts were high. However, our third hypothesis (H3) on the precipitation features driving the response characteristics of the springs cannot be accepted. In fact, the intensity and duration of EC response to precipitation events was evident and controlled by the precipitation characteristics only at the Sulden stream-like spring, where a rapid (in the order of hours) dilution and warming effect associated to the rainfall events occurred. Although a fast and transient solute dilution from rainfall has already been reported in rock glacier outflows (Krainer & Mostler, 2002; Krainer et al., 2007; Harrington et al., 2018), our study is the first to provide a measure of the intensity and duration of these responses, suggesting a threshold of 5 mm rainfall after which the increase of rainfall strongly correlates with an increased effect on EC and water temperature. The positive thermal response to rainfall (during snow free periods) at Sulden, which is unique in the literature (Krainer & Mostler, 2002; Krainer et al., 2007; Geiger et al., 2014; Krainer et al., 2015; Winkler et al., 2016; Harrington et al., 2018; Colombo et al., 2018a), might be promoted by the increased subsurface water flow coming from the surrounding moraine deposits that occupy part of the spring catchment. During rainfall events, water percolating the moraine sediments might mix with the rock glacier waters before outflowing at the Sulden spring, with the observed effect of dilution and warming. However, we suggest that this physical and chemical influence has a short duration, as the scarce development of these morainal debris promotes a quick water routing and hinders water retention.

At the Zay pond-like spring, a long-lasting effect of rainfall events was observed in terms of solute enrichment, with an intensity that is correlated to the volume of rainfall. However, only a few rainfall events triggered a detectable response in EC, and we could not identify the event parameters responsible for this response. A similar hydrochemical response to precipitation was described in a rock glacier pond by Colombo et al. (2018a), who concluded that rainfall events occurring during the snow free season enhance solute concentrations

because infiltrating rainfall flushes out the weathering products derived from permafrost thaw.

5.5. Potential drivers of contrasting hydrological patterns in rock glacier outflows

Building on previous studies, we suggest that the distinction between stream-like and pond-like systems might be a good predictor of physical and chemical patterns at multiple timescales in rock glacier waters (Figure 8) arising from different hydromorphological settings.

Stream-like springs, such as the one at Sulden, emerge and flow in defined channels. Their solute concentrations exhibit an asymptotic behaviour as summer progresses, and drop as a function of snowmelt cycles and rainfall events (Figure 8A). The Sulden rock glacier lays on steep slopes and this might promote a quick water routing across a steep sub-permafrost aquifer (according to Wagner et al., 2020). An efficient mixing of this groundwater baseflow with the rainfall/snowmelt water (which has previously crossed the unsaturated layer by lateral flow) would result in the solute dilution that we observed at the spring after rainfall events and snowmelt cycles. Intra-permafrost flow may become active during autumn, when the 0° isotherm is at its maximum depth within the active layer. In this period, most of the infiltrating water can be routed at greater depths and recharge the sub-permafrost aquifer, instead of being quickly exported across the supra-permafrost flow and smoothing the response of EC to rainfall events. At the same time, the weathering products resulting from permafrost thaw would be released into the bulk sub-permafrost flow and be exported as baseflow from the rock glacier.

In contrast, at pond-like springs (such as the one at Zay) solute concentrations peak during late summer, rarely increase after rainfall events, and are not influenced by snowmelt cycles (Figure 8B). A prevalence of slow and distributed water pathways in the rock glacier interior might cause a buffered hydrological behaviour that we observed at the pond-like spring (Winkler et al., 2016; Harrington et al., 2018). The Zay rock glacier has a gentle slope for most of its longitudinal profile, the water velocity at the spring is very low, and a wet meadow with raised grass tufts located in the rock glacier forefields indicates a diffuse water table emergence (Hayashi, 2020). The presence of a ponding system reveals the emergence of the aquifer close to the rock glacier front. Displacement (translatory flow; see Sprenger et al., 2019) and/or uplifting mechanisms (e.g., transmissivity feedback; Bishop, Seibert, Köhler & Laudon, 2004) have been suggested as key processes promoting the outflowing of old groundwater during rainfall events in aquifers and have been also suggested to occur in periglacial taluses (Muir, Hayashi & McClymont; 2011). These hydrological processes would explain the solute enrichment occurring after rainfall events at the Zay ponding spring, particularly during the window of permafrost thaw when the rock glacier aquifer is enriched in solutes that are flushed from the intra-permafrost layer.

Unfortunately, these hypotheses linked to contrasting geomorphological settings are supported by few studies, and the hydrological regime and internal structure of the Zay and Sulden rock glaciers are still unknown. Further research involving hydrological, hydrochemical, and geophysical characterisation of rock glaciers is necessary to better elucidate the linkages between the internal structure of these landforms and their

hydrochemical behaviour at multiple timescales, as well as to verify the existence of these two major systems featuring distinct hydrological dynamics.

6. CONCLUSIONS

This study details the seasonal trends in water temperature and solute concentrations of rock glacier springs and, to the best of our knowledge, represents the first attempt to quantitatively describe the fluctuation of these parameters at multiple timescales, including the effects from precipitation events. Our results provide additional insights on the importance of hydromorphological settings in driving the physical and chemical attributes of rock glacier outflows. The seasonality of these springs is dictated by the dilution effect from melting snow paralleled by an increasing influence from internal ice melt, resulting in continuously cold waters and increasing concentrations of major ions and trace elements as summer progresses. Based on the limited literature, we hypothesized that the distinct patterns of water routing determine the hydrochemical behaviour of rock glacier outflows. Stream-like springs with channelised base flow pathways display diel cycles of water parameters, and rainfall events cause solute dilution because the rainwater is efficiently routed across the rock glacier. In contrast, pond-like springs, relying on a shallow and distributed aquifer, have smoothed diel cycles of water parameters, and react slowly to changing atmospheric conditions in particular rainfall. These events can trigger solute enrichment, likely promoted by displacement or uplifting mechanisms occurring in the rock glacier aquifer. A seasonal window of major permafrost thaw can be detected for these rock glacier springs because of the efficient export of weathering products during this period.

Given the increasing hydrological influence of rock glaciers in deglaciating and glacier-free catchments, a better understanding of the drivers for distinct physical and hydrochemical patterns would help inform the management of water resources under ongoing climate change. For example, drinking water monitoring might be intensified during the window of permafrost thaw for pond-like springs, with less frequent water quality testing needed in autumn and winter. In contrast, stream-like rock glacier springs might be of greater concern given the prolonged seasonal persistence of high solute concentrations in these waters. These differing patterns might also be ecologically relevant since the enrichment of heavy metals might hinder the survival of cold-adapted species that are also sensitive to water contamination.

7. REFERENCES

Autonomous Province of Bolzano/Bozen [APB] (2020a). Online Geobrowser v.3. http://gis2.provinz.bz.it/geobrowser/?project=geobrowser_pro&view=geobrowser_pro_atlas-b&locale=it

Autonomous Province of Bolzano/Bozen [APB] (2020b). Historical series from the Civil Protection Agency. 2016/2019 period.

Baird, R., & Bridgewater, L. (2017). Standard methods for the examination of water and wastewater. 23rd edition. Washington, D.C.: American Public Health Association

Berger, J., Krainer, K., & Mostler, W. (2004). Dynamics of an active rock glacier (Ötztal Alps, Austria). *Quaternary Research*, *62*(3), 233–242. DOI: 10.1016/j.yqres.2004.07.002

Bishop, K., Seibert, J., Köhler, S. and Laudon, H. (2004), Resolving the Double Paradox of rapidly mobilized old water with highly variable responses in runoff chemistry. *Hydrological Processes*, *18*, 185-189. DOI: :10.1002/hyp.5209

Brighenti, S., Tolotti, M., Bruno, M. C., Engel, M., Wharton, G., Cerasino, L., Mair, V., & Bertoldi, W. (2019a). After the peak water: the increasing influence of rock glaciers on alpine river systems. *Hydrological Processes*, *33*(21), 1–20. DOI: 10.1002/hyp.13533

Brighenti, S., Tolotti, M., Bruno, M. C., Wharton, G., Pusch, M. T., & Bertoldi, W. (2019b). Ecosystem shifts in Alpine streams under glacier retreat and rock glacier thaw: a review. *Science of the Total Environment*, *675*, 542–559. DOI: 10.1016/j.scitotenv.2019.04.221

Brighenti, S., Tolotti, M., Wharton, G., Bertoldi, W., & Bruno, M. C. (2020). Rock glaciers and paraglacial features influence stream invertebrates in a deglaciating Alpine area. *Freshwater Biology*, 2020:00, 1-14. DOI: 10.1111/fwb.13658

Brighenti S., Hotaling, S., Finn, D.S., Fountain, A.G., Hayashi, M., Herbst, D., Saros, J.E., Tronstad, L.M., & Millar, C.I. (2021). Rock glaciers and related cold rocky landforms: Overlooked climate refugia for mountain biodiversity. *Global Change Biology*, 2021;00:1–14. DOI: 10.1111/gcb.15510

Caine, N. (2010). Recent hydrologic change in a Colorado alpine basin: an indicator of permafrost thaw? *Annals of Glaciology*, *51*(56):130–134. DOI: 10.3189/172756411795932074

Carturan, L., Zuecco, G., Seppi, R., Zanoner, T., Borga, M., Carton, A., & Dalla Fontana, G. (2016). Catchment-Scale Permafrost Mapping using Spring Water Characteristics: Catchment-Scale Permafrost Mapping using Spring Water Characteristics. *Permafrost and Periglacial Processes*, *27*(3), 253–270. DOI: 10.1002/ppp.1875

Colombo, N., Gruber, S., Martin, M., Malandrino, M., Magnani, A., Godone, D., Freppaz, M., Fratianni, S., & Salerno, F. (2018a). Rainfall as primary driver of discharge and solute export from rock glaciers: The Col d'Olen Rock Glacier in the NW Italian Alps. *Science of the Total Environment*, *639*, 316–330. DOI: 10.1016/j.scitotenv.2018.05.098

Colombo, N., Salerno, F., Gruber, S., Freppaz, M., Williams, M., Fratianni, S., & Giardino, M. (2018b). Review: Impacts of permafrost degradation on inorganic chemistry of surface fresh water. *Global and Planetary Change*, *162*, 69–83. DOI: 10.1016/j.gloplacha.2017.11.017

Colombo, N., Salerno, F., Martin, M., Malandrino, M., Giardino, M., Serra, E., … Said-Pullicino, D. (2019). Influence of permafrost, rock and ice glaciers on chemistry of high-elevation ponds (NW Italian Alps). *Science of the Total Environment*, *685*, 886–901. DOI: 10.1016/j.scitotenv.2019.06.233

Eder, M. (2019). *Origin of arsenic concentration in spring waters of relict rock glacier springs in alpine headwaters of the Seckauer Tauern Range (Austria).* Master Thesis, Graz University of Technology, 89 pp.

Engel M., Penna D., Bertoldi G., Vignoli G., Tirler W., & Comiti F. (2019). Controls on spatial and temporal variability in streamflow and hydrochemistry in a glacierized catchment. *Hydrology and Earth System Sciences*, 23, 2041–2063. DOI: 10.5194/hess-23-2041-2019

EPA – United States Environmental Protection Agency (2018). *2018 Edition of the Drinking Water Standards and Health Advisories Tables*. Office of Water U.S. Environmental Protection Agency, Washington, DC

EU – European Union (2020). *Directive (EU) 2020/2184 of the European Parliament and of the Council of 16 December 2020 on the quality of water intended for human consumption (recast)*. Official Journal of the European Union. L 435/1.

Geiger, S. T., Daniels, J. M., Miller, S. N., & Nicholas, J. W. (2014). Influence of Rock Glaciers on Stream Hydrology in the La Sal Mountains, Utah. *Arctic, Antarctic, and Alpine Research*, *46*(3), 645–658. DOI: 10.1657/1938-4246-46.3.645

Haeberli, W., Schaub, Y., & Huggel, C. (2016). Increasing risks related to landslides from degrading permafrost into new lakes in de-glaciating mountain ranges. *Geomorphology*, *293*, 405-417. DOI: 10.1016/j.geomorph.2016.02.009

Harrington, J. S., Hayashi, M., & Kurylyk, B. L. (2017). Influence of a rock glacier spring on the stream energy budget and cold-water refuge in an alpine stream. *Hydrological Processes*, *31*(26), 4719–4733. DOI: 10.1002/hyp.11391

Harrington, J. S., Mozil, A., Hayashi, M., & Bentley, L. R. (2018). Groundwater flow and storage processes in an inactive rock glacier. *Hydrological Processes*, *32*, 3070-3088. DOI: 10.1002/hyp.13248

Hayashi, M. (2020). Alpine hydrogeology: the critical role of groundwater in sourcing the headwaters of the World. *Groundwater*. DOI:10.1111/gwat.12965

Husson, F., Josse, J., Le, S., & Mazet, J. (2020). Factominer: Multivariate Exploratory Data Analysis and Data Mining. R package version 2.3. http://factominer.free.fr

IBM (2018). SPSS Statistics software, v.26

IPCC - Intergovernmental Panel on Climate Change (2019). IPCC Special Report on the Ocean and Cryosphere in a Changing Climate. Geneva, Switzerland

Jones, D. B., Harrison, S., Anderson, K., & Betts, R. A. (2018). Mountain rock glaciers contain globally significant water stores. *Scientific Reports*, 1-10. DOI: 10.1038/s41598-018-21244-w

Jones, D. B., Harrison, S., Anderson, K., & Whalley, W. B. (2019). Rock glaciers and mountain hydrology: a review, *Earth-Science Reviews*, *193*, 66–90. DOI: 10.1016/j.earscirev.2019.04.001

Kassambara, A. & Mundt, F. (2020). Factoextra: Extract and Visualize the Results of Multivariate Data Analyses. R package version 1.0.7. https://CRAN.R-project.org/package=factoextra

Khamis, K., Brown, L. E., Milner, A. M., & Hannah, D. M. (2015). Heat exchange processes and thermal dynamics of a glacier-fed alpine stream. *Hydrological Processes*, *29*, 3306-3317. DOI: 10.1002/hyp.10433

Kofler, C., Steger, S., Mair, V., Zebisch, M., Comiti, F., & Schneiderbauer, S. (2020). An inventory-driven rock glacier status model (intact vs. relict) for South Tyrol, Eastern Italian Alps. *Geomorphology*, *350*, 106887. DOI: 10.1016/j.geomorph.2019.106887

Krainer, K. (2011). Hydrological discharge measurements, geophysical measurements for assessing the ice content of permafrost phenomena. WP7 Water resources – action 7.2 report. PermaNET project. Retrieved from http://www.permanet-alpinespace.eu/archive/pdf/WP7_2.pdf

Krainer, K. & Mostler, W. (2002). Hydrology of active rock glaciers: examples from the Austrian Alps. *Arctic, Antarctic, and Alpine Research*, *34*(2), 142. DOI: 10.2307/1552465

Krainer, K., Mostler, W. & Spötl, C. (2007). Discharge from active rock glaciers, Austrian Alps: a stable isotope approach. *Austrian Journal of Earth Sciences*, *100*, 102-112.

Krainer, K., Chinellato, G., Tonidandel, D., & Lang, K. (2011). *Analysis of the contribution of permafrost ice to the hydrological water regime*. WP7 Water resources – action 7.3 report. PermaNET project. Retrieved from http://www.permanet-alpinespace.eu/archive/pdf/WP7_3.pdf

Krainer, K., Bressan, D., Dietre, B., Haas, J. N., Hajdas, I., Lang, K., … Tonidandel, D. (2015). A 10,300-year-old permafrost core from the active rock glacier Lazaun, southern Ötztal Alps (South Tyrol, northern Italy). *Quaternary Research*, *83*(2), 324–335. DOI: 10.1016/j.yqres.2014.12.005

Landwehr, J.M., & Coplen, T.B. (2006). *Line-conditioned excess: a new method for characterizing stable hydrogen and oxygen isotope ratios in hydrologic systems*. In Isotopes in Environmental Studies, Aquatic Forum 2004, International Atomic Energy Agency, IAEA-CSP-26, 132 – 135.

Leopold, M., Williams, M.W., Caine, N., Völkel, J., & Dethier, D. (2011). Internal structure of the Green Lake 5 rock glacier, Colorado Front Range, USA. *Permafrost and Periglacial Processes*, *22* (2), 107–119. DOI: 10.1002/ppp.706

Millar, C. I., Westfall, R. D., & Delany, D. L. (2013). Thermal and hydrologic attributes of rock glaciers and periglacial talus landforms: Sierra Nevada, California, USA. *Quaternary International*, *310*, 169–180. DOI: 10.1016/j.quaint.2012.07.019

Montrasio, A., Berra, F., Cariboni, M., Ceriani., M., Deichmann, N., Longhin, M., … Zappone, A. (2015). Note illustrative della Carta Geologica d'Italia, Foglio 024-Bormio. ISPRA-SGI-Regione Lombardia

Molina-Sanchis, I., Lázaro, R., Arnau-Rosalén, E., & Calvo-Cases, A. (2016). Rainfall timing and runoff: The influence of the criterion for rain event separation. *Journal of Hydrology and Hydromechanics*, *64*(3), 226-236. DOI: 10.1515/johh-2016-0024

Morlet, J., Arens, G., Fourgeau, E., & Giard, D. (1982). Wave propagation and sampling theory—Part I: Complex signal and scattering in multilayered media. *Geophysics* 47 (2), 203–221. DOI: 10.1190/1.1441328

Muir, D. L., Hayashi, M., & McClymont, A. F. (2011). Hydrological storage and transmission characteristics of an alpine talus. *Hydrological Processes*, *25*(19), 2954–2966. DOI: 10.1002/hyp.8060

Munroe, J. S. (2018). Distribution, evidence for internal ice, and possible hydrologic significance of rock glaciers in the Uinta Mountains, Utah, USA. *Quaternary Research*, *90*, 50–65. DOI: 10.1017/qua.2018.24

Nickus, U., & Thies, H. (2015). L'effetto dello scioglimento del permafrost sulla chimica dell'acqua. In Mair V., Lang K., Tonidandel D., Thaler B., Alber R., Lösch B., … Tolotti M. (Eds.). *Progetto Permaqua – Permafrost e il suo effetto sul bilancio idrico e sull'ecologia delle acque di alta montagna* (pp. 14-15). Provincia Autonoma di Bolzano, Bolzano, Italy: Ufficio geologia e prove dei materiali

R Development Core Team (2020). R: a language and environment for statistical computing. R Foundation for Statistical Computing, Vienna, Austria. https://www.R-project.org/

Rösch, A., & Schmidbauer, H. (2018). WaveletComp: Computational Wavelet Analysis. R package version 1.1.

Scapozza, C., Deluigi, N., Bulgheroni, M., Pera Ibarguren, S., Pozzoni, M., Colombo, L., & Lepori, F. (2020). Assessing the impact of ground ice degradation on high mountain lake environments (Lago Nero catchment, Swiss Alps). *Aquatic Sciences, 82*(5). DOI: 10.1007/s00027-019-0675-7

Schoeneich, P., Lieb, G. K., Kellerer-Pirklbauer, A., Deline, P., & Pogliotti, P. (2011). Chapter 1: Permafrost response to climate change. In Kellerer-Pirklbauer, A. et al. (Eds): *Thermal and geomorphic permafrost response to present and future climate change in the*

European Alps. PermaNET project, final report of Action 5.3. On-line publication ISBN: 978-2-903095-58-1

Sprenger, M., Stumpp, C., Weiler, M., Aeschbach, W., Allen, S.T., Benettin, P., … & Werner, C. (2019). The Demographics of Water: A Review of Water Ages in the Critical Zone. *Reviews of Geophysics*, *57*, 1–35. DOI: 10.1029/2018RG000633

Steingruber, S. M., Bernasconi, S. M., & Valenti, G. (2020). Climate Change-Induced Changes in the Chemistry of a High-Altitude Mountain Lake in the Central Alps. *Aquatic Geochemistry*. DOI: 10.1007/s10498-020-09388-6

Thies, H., Nickus, U., Mair, V., Tessadri, R., Tait, D., Thaler, B., & Psenner, R. (2007). Unexpected response of high Alpine Lake waters to climate warming. *Environmental Science & Technology*, *41*(21), 7424–7429. DOI: 10.1021/es0708060

Tolotti, M., Cerasino, L., Donati, C., Pindo, M., Rogora, M., Seppi, R., & Albanese, D. (2020). Alpine headwaters emerging from glaciers and rock glaciers host different bacterial communities: Ecological implications for the future. *Science of the Total Environment*, *717*, 137101. DOI: 10.1016/j.scito tenv.2020.137101

US Army Corps of Engineers, North Pacific Division (1956). Snow Hydrology; Summary Report of the Snow Investigation. Portland, Oregon.

Wagner, T., Pauritsch, M., & Winkler, G. (2016). Impact of relict rock glaciers on spring and stream flow of alpine watersheds: examples of the Niedere Tauern Range, Eastern Alps (Austria). *Austrian Journal of Earth Sciences*, *109*, 117-131. DOI: 10.17738/ajes.2016.0006

Wagner, T., Brodacz, A., Krainer, K., & Winkler, G. (2020). Active rock glaciers as shallow groundwater reservoirs, Austrian Alps. *Grundwasser – Zeitschrift der Fachsection Hydrogeologie*. DOI: 10.1007/s00767-020-00455-x

Wei, T. (2017). Corrplot: Visualization of a Correlation Matrix. R package version 0.84. https://github.com/taiyun/corrplot

Williams, M. W., Knauf, M., Caine, N., Liu, F., & Verplanck, P. L. (2006). Geochemistry and source waters of rock glacier outflow, Colorado Front Range. *Permafrost and Periglacial Processes*, *17*, 13–33. DOI: 10.1002/ppp.535

Winkler, G., Wagner, T., Pauritsch, M., Birk, S., Kellerer-Pirklbauer, A., Benischke, R., … Hergarten, S. (2016). Identification and assessment of groundwater flow and storage components of the relict Schöneben Rock Glacier, Niedere Tauern Range, Eastern Alps (Austria). *Hydroegeology Journal*, *24*, 937–953. DOI: 10.1007/s10040-015-1348-9

Wood, S. N. (2020). Mixed GAM Computation Vehicle with Automatic Smoothness Estimation. R package version 1.8-33. https://CRAN.R-project.org/package=mgcv

Zuur, A. F., Ieno, E. N., Walker, N., Saveliev, A. A., & Smith, G. (2009). Mixed effects models and extensions in ecology with R. Springer

Data Availability statement

The data supporting our findings are available upon reasonable request to the corresponding author.

Conflict of Interest Statement

The authors declare no conflict of interest.

Figure 1. Main features of the study sites. A) Geographical location of the Zay and Sulden/Solda subcatchments in the European Alps; the two areas are separated by the Rosim subcatchment (not highlighted in the figure); B) Location in a DEM map of the Zay (ZRG) and C) Sulden spring. D-E) Pictures of the sites with spring locations highlighted. F) Weather conditions at the Madriccio/Madritsch station (APB, 2020b). Monthly values for: total precipitation (Prec., in mm, black columns), average snow cover thickness (snow, in cm, grey area) and average air temperature (T_{air}, °C, black line) during different years (that are separated by dotted vertical lines). The snow free seasons, when only transient snow events occurred, are highlighted in green bars. The accumulation of winter snow started on the 10th October in 2016 (not shown). Vertical black arrows indicate the sampling dates.

Figure 2. A) PCA biplot with varimax rotation. Ellipses group the samples of the two springs (continuous line = ZRG, dashed line = SRG). B) Correlation matrix of the selected variables, with Pearson values represented by different colours (blue = positive correlation, red = negative correlation). Colour intensity and circle size represent the correlation strength (pale and small = weak, intense and large = strong). Blank cells correspond to correlations that are not significant ($p > 0.01$).

Figure 3. Trends of stable water isotopes. A) Dual-isotope plot for water samples of precipitation, snowmelt water, ice melt and spring water at the two springs. Local (LMWL in black; $\delta^2H = 7.8\ \delta^{18}O + 16.9$) and Global (GMWL in red; $\delta^2H = 8.2\ \delta^{18}O + 11.27$) Meteoric Water Lines are plotted. The close-up box highlights the plot area where the spring samples are located in the dual plot. Scatterplots of B) isotopic values (δ^2H) and C) line-conditioned excess (lc-excess) as a function of the days after the snowmelt variable. D) boxplots of lc-excess for precipitation, ice melt, and snowmelt water samples, with the same axis scale and centring as in C) to facilitate comparison. Notes: points for precipitation refer to multiple events that occurred during two weeks to one month and collected on the day of reference. Interpolation lines are based on polynomial regression (level three for green-ZRG, level two for black-SRG). Values of δ^2H and $\delta^{18}O$ are expressed in ‰ (against the Vienna Standard Mean Ocean Water).

Figure 4. Seasonal trends of water parameters over summer, as a function of the days after the snowmelt end (reference Madriccio/Madritsch station, APB; 2020) at SRG (left panels) and ZRG (right panels). In each scatterplot, distinct parameters are shown in different colours and shapes, and their scale corresponds to that of the axis where the name of each parameter is placed. Interpolation lines represent linear regression or polynomial smoothing curves of level three (turbidity at SRG, smoothing curves for ZRG).
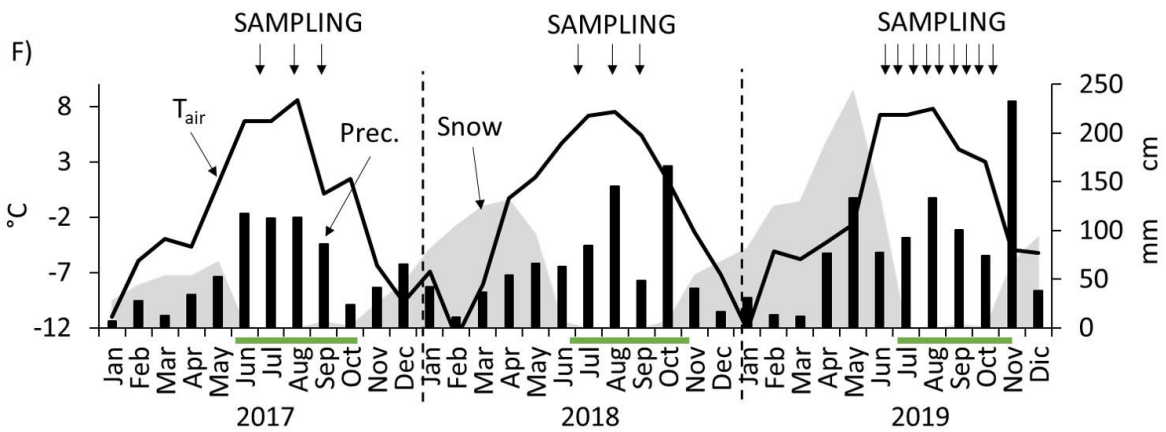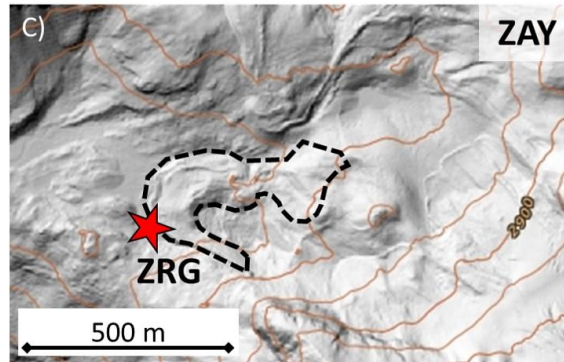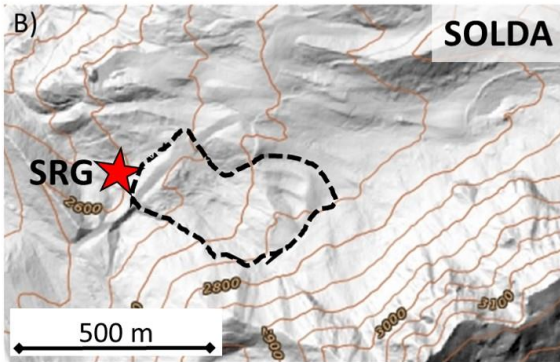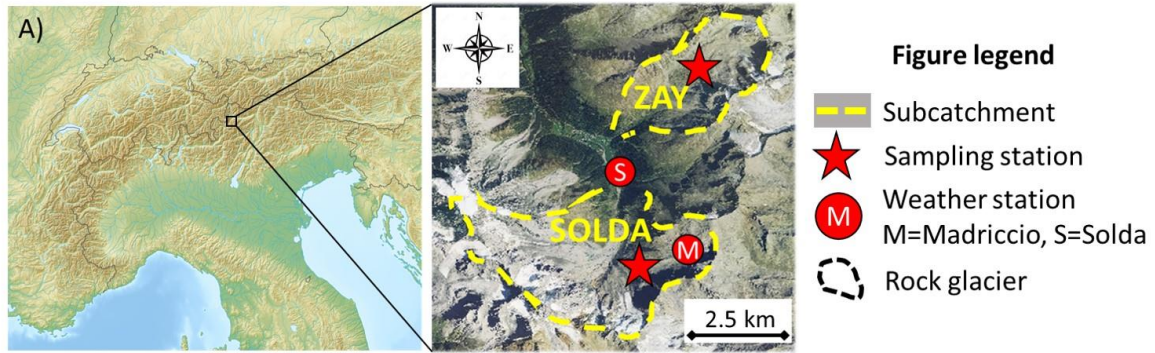
Figure 5. A) Series of EC and T_{water} (daily average) at the two springs over the logging period (24th June – 20th September 2017, 9th June – 26th September 2018, 18th June – 15th October 2019). As a reference, we provide the daily values of air temperature and total precipitation, and the presence of snow cover at the Madriccio/Madritsch station (Source: APB, 2020b). B) Model fit of GAMs analyses performed with T_{water} and EC in the two springs, setting the days

after the snowmelt as a smoothing term (see Table 3 for model numerical results). Solid line is the smoother, shaded area represents 95 % confidence interval.
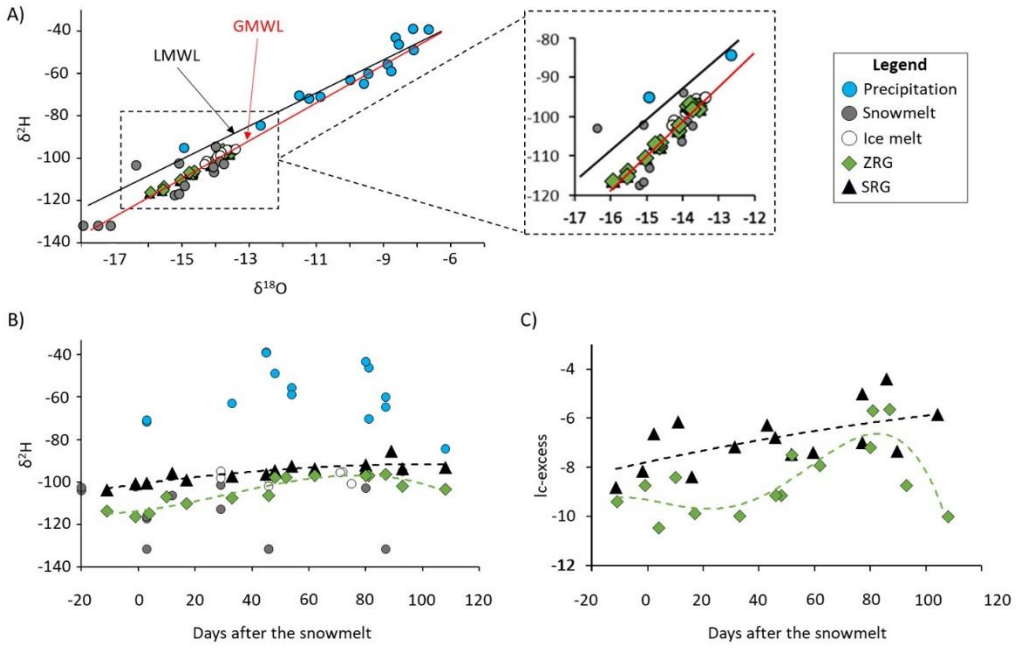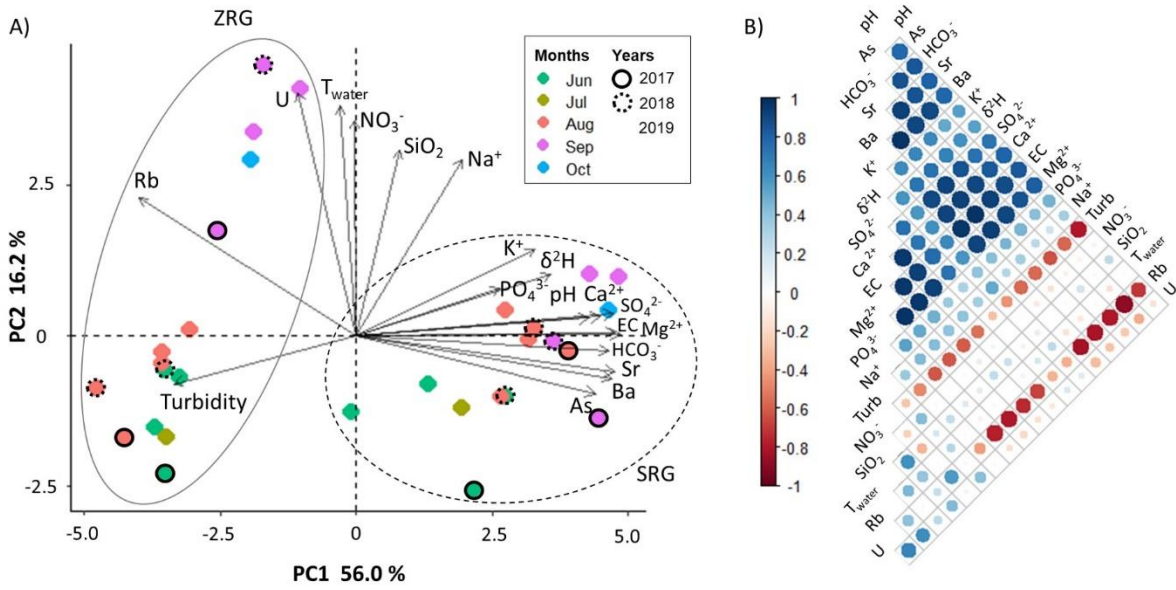
Figure 6. Wavelet power spectrum of electrical conductivity and water temperature recorded at SRG and ZRG during each summer. As a reference, the daily values of air temperature (°C, black line), snow height (cm, grey area) and total precipitation (mm, grey bars) at the Madriccio/Madritsch station are plotted in the centre of the figure (Source: APB, 2020b). Horizontal axes represent the timeline, shown only in the plot of weather conditions. Vertical axes indicate the fluctuation period (days). The wavelet power spectrum (coloured space, 250 power levels) represents the affinity of each variable to each period over the series. White contours delineate the areas of significant periods ($p < 0.01$, method "white noise"), and the black line indicates a ridge in the power spectrum (i.e., strongest affinity of the variable with the corresponding period).

Figure 7. Scatterplots of precipitation parameters vs. the associated response of water conditions at the two springs. We fitted 95 % confidence intervals of linear (LM) and Generalised Additive (GAM) models. Red points indicate the values that were discarded from the models because snow cover was present (Precipitation-δEC plot) or because T_{air} was low (< 4 °C; Precipitation-δT plot) during the event.
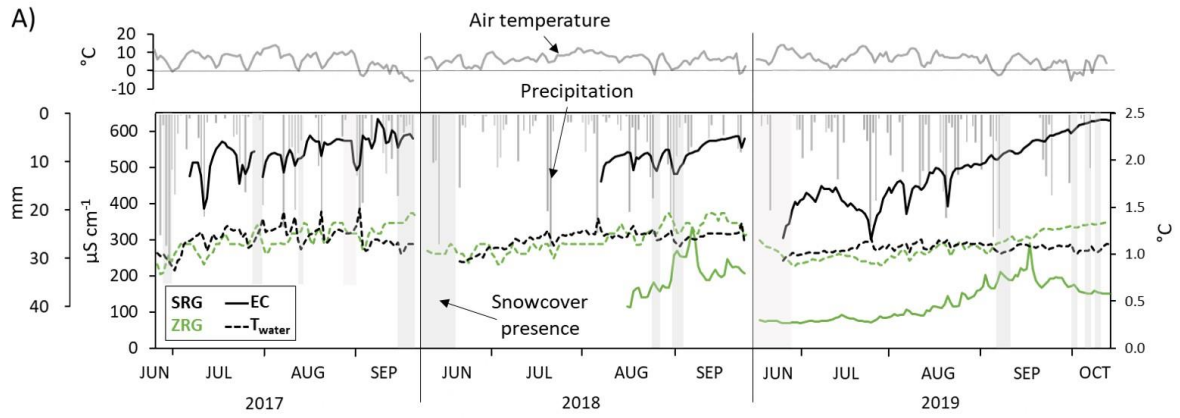
Figure 8. Schematic representation of the distinct behaviour of rock glacier springs at multiple timescales during the snow free season. A) Stream-like springs such as the Sulden one exhibit an asymptotic behaviour of solute concentrations as summer progresses (A_1). Rainfall events (arrows, thickness, and length indicate increasing precipitation amount) cause a rapid dilution effect (A_2) at these springs, where diel fluctuations of solute concentrations are evident soon after the snowmelt period, and progressively smooth towards the end of the summer (A_3). B) Pond-like springs such as the Zay one exhibit a unimodal behaviour of solute concentrations as summer progresses (B_1), with peaks corresponding to the window of permafrost thaw (WPT). Rainfall events can cause a delayed and long-lasting effect of solute enrichment (B_2) at these springs where diel fluctuations of solute concentrations do not occur (B_3). Callouts indicate the number of studies supporting this evidence (see main text for references).
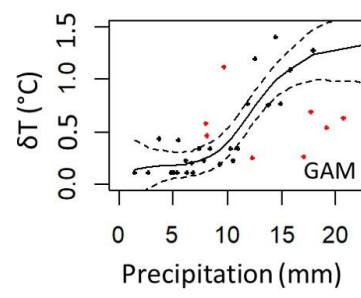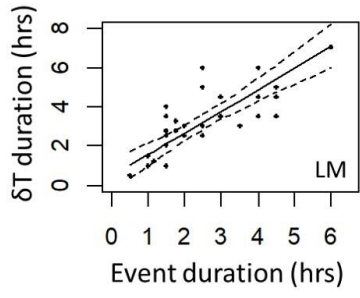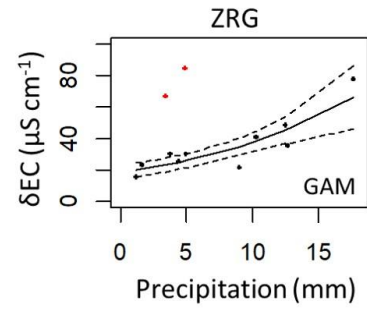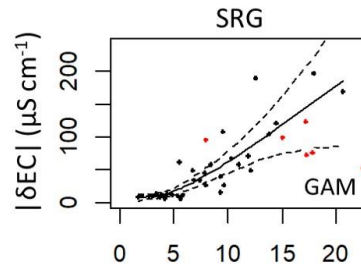
SRG ZRG

Days after the snowmelt   Days after the snowmelt

A)

B) SRG

WATER TEMPERATURE   ELECTRICAL CONDUCTIVITY

ZRG

WATER TEMPERATURE   ELECTRICAL CONDUCTIVITY

Days after the snowmelt

Days after the snowmelt

2017   2018   2019

Water temperature

SRG

ZRG

Electrical conductivity

SRG

ZRG

Legend

WAVELET POWER
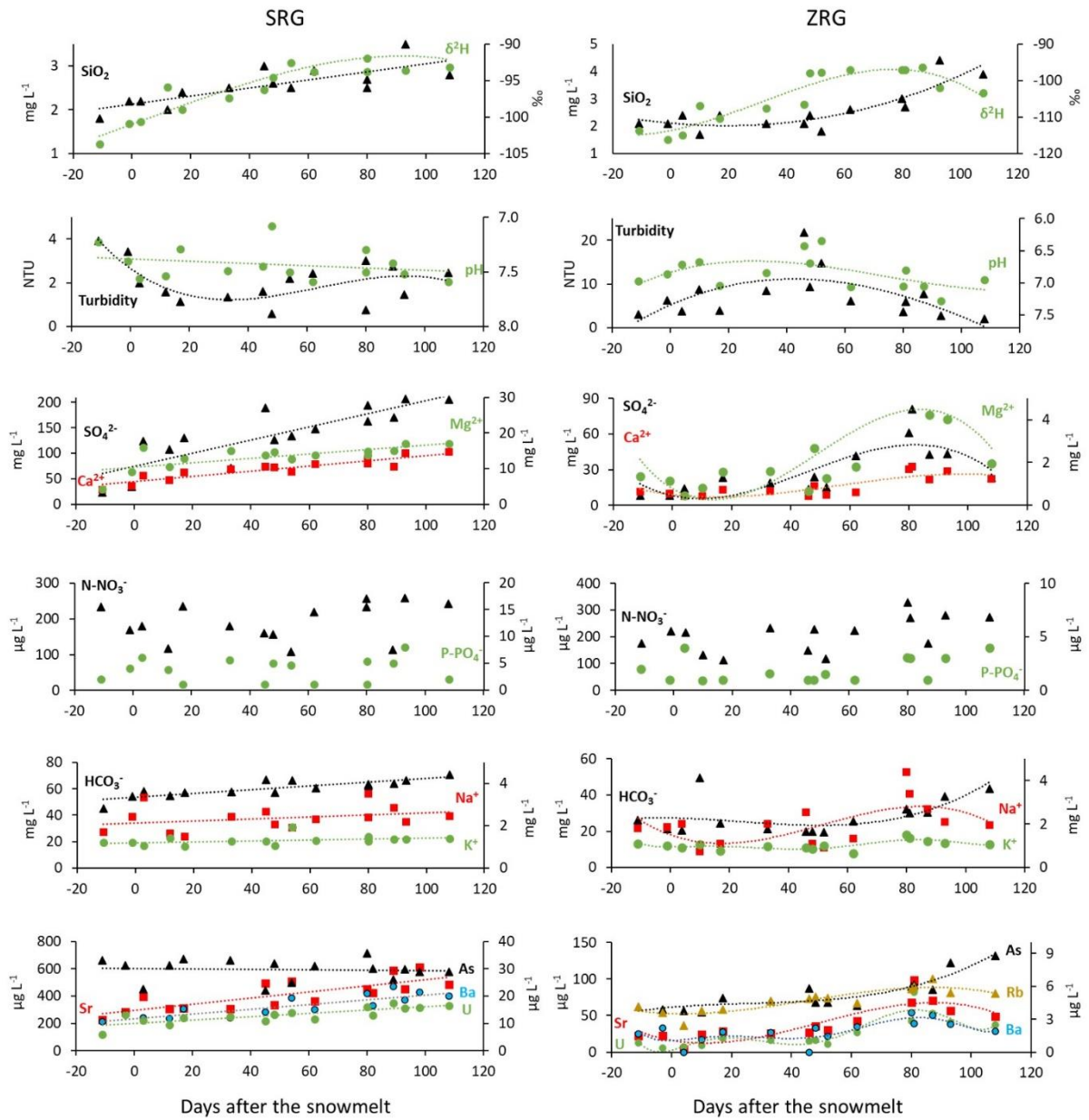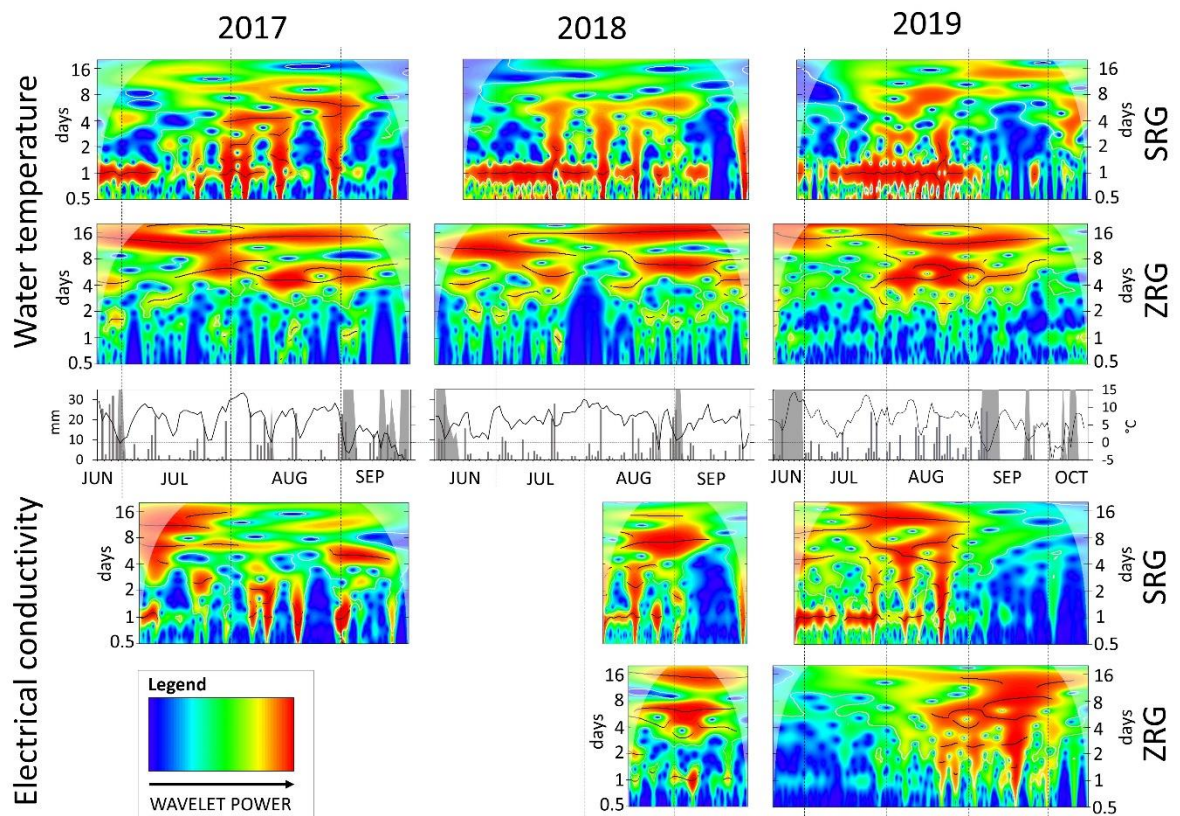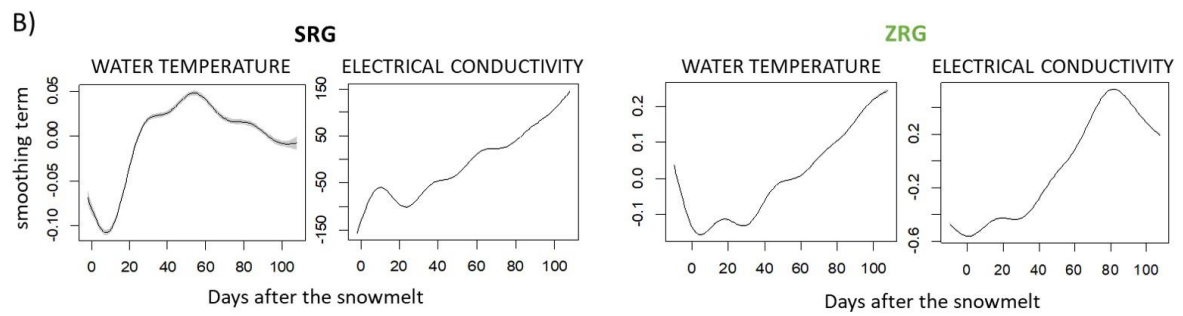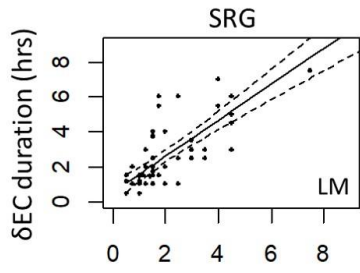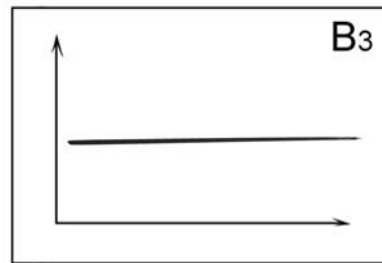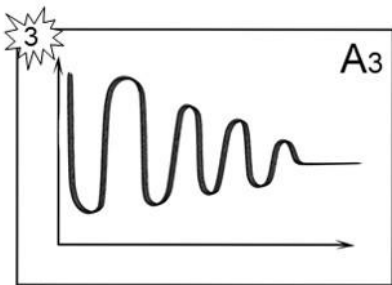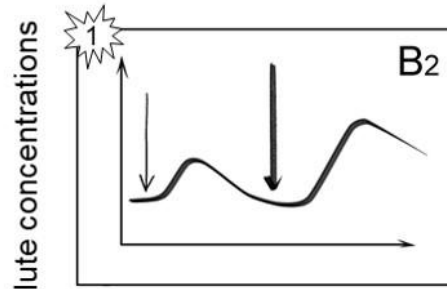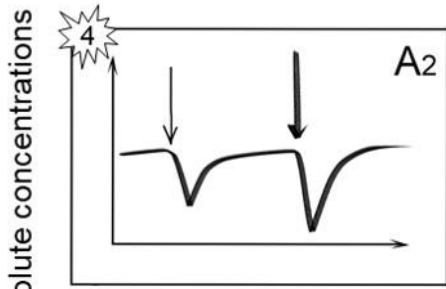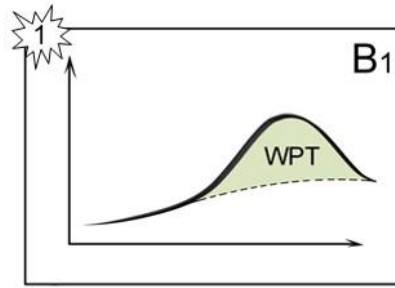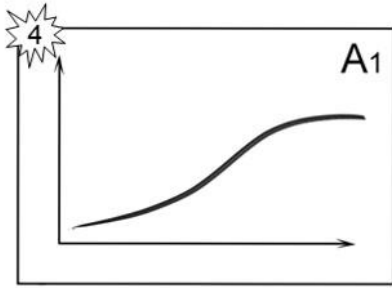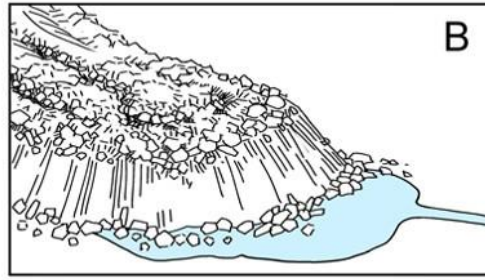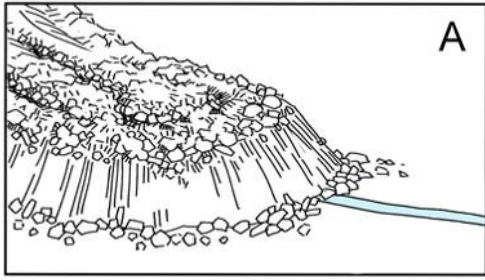
Table 1. Characteristics of the Sulden and Zay rock glaciers, and their studied springs. Morphometric features were calculated from APB (2020a). [a] Rock glacier lithology was estimated by visual inspection at the rock glacier front, and thus the % values of bedrock constituents represent a rough estimate. [b] A siderite with manganese ore (~1-2 m thick) crosses sub-horizontally the upper cliffs of the Zay subcatchment (Mair, pers. comm, 2019). [c] calculated along the first ten meters of the stream. Water velocity was recorded with a hand probe (see Brighenti et al., 2020).

Rock glaciers	Sulden	Zay
Elevation range (m a.s.l.)	2620-2765	2719-2820
Area (m^2)	120 000	88 000
Maximum length and width (m)	450, 360	563, 266
Front maximum height (m)	20	10
Front maximum steepness (%)	78	45
Average surface steepness (%)	35	18
Lithology of rocky debris [a]	Quartzphyllites (40%), michaschists (30%), orthogneisses (30%), sporadic andesites	Orthogneisses (70%), quartzphyllites (30%) [b]
Springs	**SRG**	**ZRG**
Elevation (m a.s.l.)	2600	2719
Channel slope (%) [c]	20	< 1
Catchment area (m^2)	330 000	355 000
Catchment occupied by rock glacier (%)	36	24.8
Average slope of upstream catchment (%)	44	28
Water velocity (m/s) [c]	0.4-0.6	0.1-0.2
Discharge (L/s) [c]	29-46	28-173

Table 2. Variable loadings of the physical and chemical variables in the principal component analysis. Bold numbers indicate strong correlation (< -0.6 or > 0.6)

	PC1	PC2
EC	**0.99**	0.01
Mg^{2+}	**0.97**	0.02
Sr	**0.97**	-0.11
Ba	**0.96**	-0.14
Ca^{2+}	**0.96**	0.08
HCO_3^-	**0.95**	-0.05
SO_4^{2-}	**0.91**	0.07
As	**0.90**	-0.19
pH	**0.88**	0.04
Rb	**-0.82**	0.46
δ^2H	**0.73**	0.22
Turbidity	**-0.68**	-0.16
K^+	**0.66**	0.27
$P-PO_4^{3-}$	**0.55**	0.18
U	-0.22	**0.82**
T_{water}	-0.07	**0.78**
$N-NO_3^-$	-0.01	**0.73**
SiO_2	0.14	**0.63**
Na^+	0.39	**0.60**

Table 3. Results from Linear Models (LM), Generalised Linear Models (GLM) and Generalised Additive Models (GAM). For each analysis we provide: the response variable; the explanatory variable (elapsed = days elapsed after the snowmelt; duration/intensity = duration/intensity of precipitation) and covariates (* = interaction term), the model type (LM, GLM, GAM); the type of distribution selected (GAM/GLM); the F-value of the smooth term (GAM) or t-value of the explanatory variable (GLM) or the F-statistic for LM; the intercept and slope values; the deviance explained (Dev.exp.) by GAM/GLM or R^2 value for LM.
[a] p-values of the intercept were always < 0.001; [b] Slope compared with 2017, only for GAM of Figure 5; [c] p-value of covariates, only for LM and GLM. [d] Data from 2017 are missing, and values for 2018 start from early August.

Response variable	Explanatory var., covariates	Model type	Distribution (link)	F/t	Intercept [a]; Slope [b]; p-value [c]	Dev.exp. / R^2
T_{water} at SRG	elapsed, year	GAM (Figure 5)	Gamma (log)	839.5	0.12; 2018 = 0.006, 2019 = -0.06	38.9 %
EC at SRG	elapsed, year	GAM (Figure 5)	Gaussian	7976	550.7; 2018 = -54.1; 2019 = -52.4	83.4 %
T_{water} at ZRG	elapsed, year	GAM (Figure 5)	Gaussian	9075	1.15; 2018 = -0.006, 2019 = -0.08	81.6 %
EC at ZRG [d]	elapsed, year	GAM (Figure 5)	Gamma (log)	17691	4.9; 2019 = -0.09	94.0 %
δEC duration at SRG	Duration	LM (Figure 7)	na	96.5	0.56; 1.0, < 0.001	0.66
δT duration at SRG	Duration	LM (Figure 7)	na	54.3	0.4; 1.12, < 0.001	0.65
|δEC| at SRG	Total precipitation, elapsed, intensity	GLM	Gamma (log)	-8.45	2.12; p > 0.71	60.3 %
δT at SRG	Total precipitation, maximum intensity, T_{air}	GLM	Gamma (log)	3.3	-1.78; p > 0.36	48 %
δT at SRG (T_{air} > 4°C)	Total precipitation	GLM	Gamma (log)	6.3	-2.4	67 %
δEC at ZRG	Total precipitation	GAM (Figure 7)	Gamma (log)	28.6	3.5	77.5 %
|δEC| at SRG	Total precipitation	GAM (Figure 7)	Gamma (identity)	14.4	2.5	74.9 %
δT at SRG	Total precipitation	GAM (Figure 7)	Gaussian	21.7	0.48	83.5 %